Elastic loading enhanced NH_3 sensing for surface acoustic wave sensor with highly porous nitrogen doped diamond like carbon film

Hao Zhu[1], Dong Xie[1], Sixu Lin[1], Wenting Zhang[1], Youwei Yang[2], Ruijie Zhang[3], Xing Shi[3], Hongyan Wang[1], Zhengquan Zhang[1,*], Xiaotao Zu[5], Yongqing Fu[4], Yongliang Tang[1,*]

[1]School of Physical Science and Technology, Southwest Jiaotong University, Chengdu, 610031, P. R. China

[2]Science and Technology on Reactor System Design Technology Laboratory, Nuclear Power Institute of China, Chengdu, 610213, P. R. China

[3]Nanjing Electronic Equipment Institute, Nanjing, 210007, P. R. China

[4]Faculty of Engineering and Environment, Northumbria University, Newcastle upon Tyne, NE1 8ST, UK

[5]School of Physics, University of Electronic Science and Technology of China, Chengdu, 610054, P. R. China

*Correspondence Authors:

Zhengquan Zhang

E-mail address: zhangzhengquan8@163.com; Telephone: +86-13882293507

Yongliang Tang

E-mail address: tyl@swjtu.edu.cn; Telephone: +86-15884573263

Abstract:

We proposed a surface acoustic wave (SAW) NH_3 gas sensor based on nitrogen doped diamond like carbon (N-DLC) film. The N-DLC film, prepared using a microwave electron cyclotron resonance plasma chemical vapor deposition (ECR-PECVD) method, is highly porous and physically and chemically stable, and have active polar groups on its surface, which can selectively absorb polar NH_3 gas molecules. These features of the film lead to the high sensitivity, low noise and excellent stability of the sensor. The sensor can achieve capabilities of *in-situ* monitoring NH_3 in a concentration range from 100 ppb to 100 ppm with fast response (~5 s) and recovery (~29 s) at room temperature. The NH_3 sensing mechanism is attributed to the decreased porosity of the N-DLC film caused by adsorbed NH_3 molecules on its polar groups, which leads an increase of the elastic modulus of the film.

Keywords: N doped DLC; surface acoustic wave (SAW); NH_3 gas sensor; elastic modulus

1. Introduction

Ammonia (NH_3) gas is toxic, and its maximum allowed concentration in working and living environments defined by Occupational Safety and Health Administration, USA, is 35 ppm [1,2]. Long-term exposure to NH_3 gas with a concentration higher than 50 ppm can lead to damage to respiratory and eyes tracts [3], and exposure to NH_3 gas with a concentration higher than 5000 ppm can cause sudden collapse or death of a person [4,5]. Besides, liquid NH_3 is flammable and may cause an explosion if its leakage happens [6-8]. For example, an explosion caused by the leaked NH_3 killed more than 100 people in Jilin, China, in 2013. Although the lower limit of human perception by smell is around 25 ppm NH_3 [5], human olfaction is often unreliable for the NH_3 detection and NH_3 concentration far below this limit should be known much earlier in many occasions [9]. Despite its extreme danger, NH_3 is vastly used in modern chemical and semiconductor industries [10-12]. Therefore, gas sensors which can *in-situ* monitoring the low concentration of the NH_3 are critical for a safe working and living environments and saving lives.

In the last decade, along with the development of the micro-electro-mechanical systems (MEMS) technology, surface acoustic wave (SAW) technique has become widely used in NH_3 sensing because surface acoustic wave is highly sensitive to physical and chemical changes of the sensing layers deposited onto the SAW device [13-16]. Semiconducting oxides and polymers are usually employed as sensing layers of SAW based NH_3 sensors, because they can effectively absorb and react with NH_3 molecules [17-19]. For example, Constantinoiu et al. reported that a SAW NH_3 sensor

using a SnO_2/Co_3O_4 bi-layer sensitive film has achieved a response of ~1 kHz toward 100 ppm NH_3 [20]. However, these semiconducting oxides and polymers often show a poor stability, which leads to the rapid degradation of sensitivity and stability of the gas sensors [21,22]. Therefore, it is crucial to explore new sensing materials which are both stable and sensitive to NH_3 gas.

Nitrogen doped DLC (N-DLC) films have attracted great interests for industrial applications mainly because of their high hardness, low friction, chemical inertness, water resistivity, wear and corrosion resistance [23,24]. Besides, they have numerous active polar terminating bonds ($-NH_x$) on their surfaces [24-26]. Previous studies revealed that these polar terminating bonds can act as the active sites for adsorption of gas molecules, such as NH_3 [27], thus leading to changes of mass, elastic modulus and electrical conductivity of N-DLC films. In addition, they often have pores in their structures, which are beneficial for gas adsorption and diffusion [28]. Their excellent properties provide a great potential to be explored as highly stable and sensitive layers for NH_3 gas sensors. Nevertheless, as far as we have searched, few reports have been focused on their NH_3 sensing applications.

In this work, we fabricated a SAW gas sensor with a sensing layer of a porous N-DLC film and investigated its sensing performance and mechanism for NH_3. Results showed that the sensor can be operated at room temperature, with high sensitivity, good linearity, selectivity, fast response, recovery and excellent stability for sensing NH_3 in the concentration range from 100 ppb to 100 ppm.

2. Materials and methods

Commercial ST-Cut quartz substrate was used for the fabrication of the SAW device. Aluminum interdigital transducers (IDTs, 50 pairs) and reflecting gratings (250 pairs) with a thickness of 200 nm were deposited on the substrate using standard photolithography and lift-off processes to fabricate the SAW resonator. The fabricated SAW resonator is shown in Fig. 1(a) and 1(b), and the transmission feature (S_{21} parameter) measured by a network analyzer (Agilent E5071C) is given in Fig. 1(c), which indicates the insertion loss and the quality factor are ~17 dB and ~4000, respectively. The central frequency of the resonator is ~200 MHz since the IDTs and reflecting gratings have a periodicity of 16 μm as shown in Figs. 1(b) and 2(a), and the acoustic wave speed on ST-cut quartz is 3158 m/s. The center-to-center distance between the IDTs is 200 wavelengths.

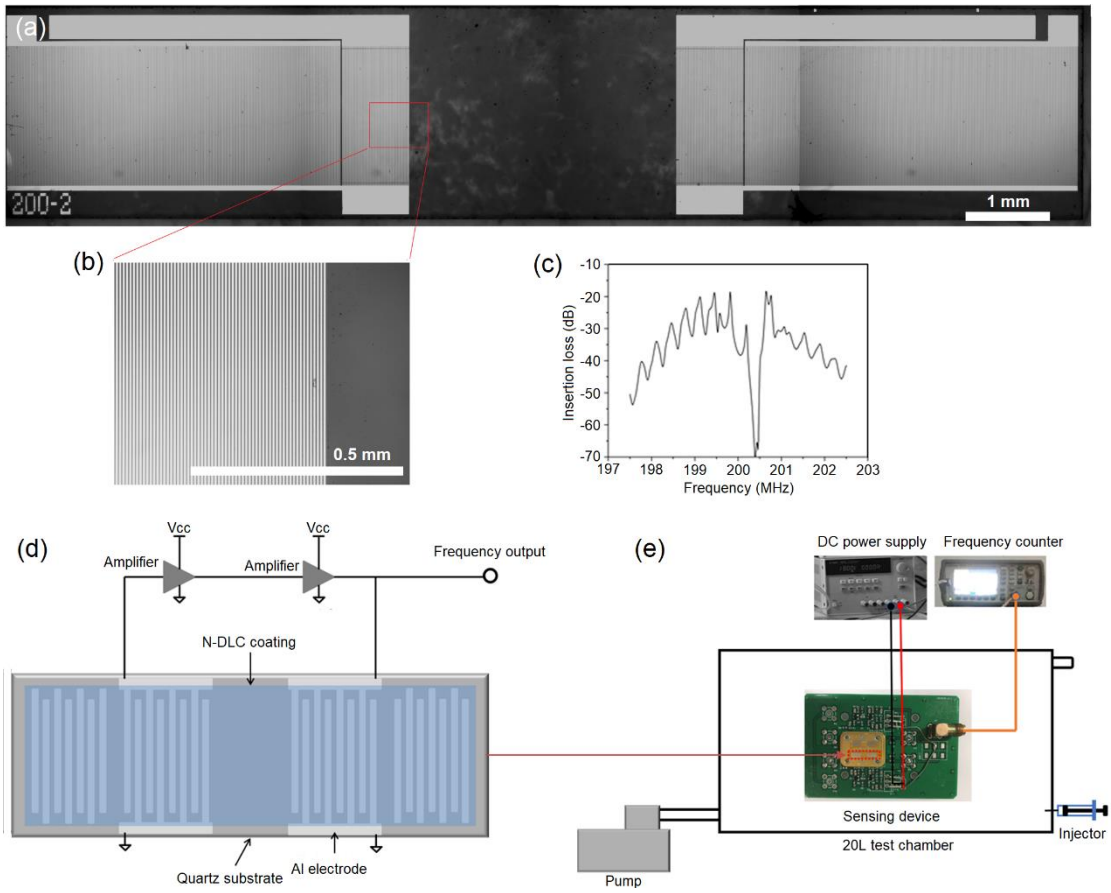

Fig. 1(a) The optical microscopy image of the SAW resonator; (b) The enlarged image of the area in the red box in (a); (c) The transmission feature (S_{21} parameter) of the SAW resonator; (d) The schematic diagram of a SAW sensor; (e) experimental setup for gas sensing measurement.

N-DLC films were deposited on the SAW resonators using a microwave electron cyclotron resonance plasma chemical vapor deposition (ECR-PECVD) method, as reported in Ref. [29]. The microwaves with a high-density plasma were generated from the upper side of the deposition chamber. A negative pulse voltage was applied on the substrate to control the energy of ions. Before the film deposition, the chamber was evacuated to 1.0×10^{-3} Pa and then argon (Ar) gas was introduced inside chamber to generate the plasma, which sputtered and cleaned the substrate (400 W microwave

power, -800 V pulse biased with frequency 15 kHz and duty ratio 30%, 20 min). Then a gas mixture of C_2H_2, N_2 and Ar were introduced into the chamber for the deposition of the N-DLC films. In this study, the microwave power, biased voltage, operating pressure and process time were maintained to be constants during the deposition, but the C_2H_2/N_2 gas flow ratios were varied. The detailed deposition parameters are listed in Table 1.

Table 1 Experimental parameters for the deposition of N-DLC film

Film No.	N_2 flow rate (sccm)	Ar flow rate (sccm)	C_2H_2 flow rate (sccm)	Microwave power (W)	Biased voltage (V)	Operating pressure (pa)	Process time (min)
#1	5	10	30	400	-800	10^{-3}	20
#2	15	10	30	400	-800	10^{-3}	20
#3	30	10	30	400	-800	10^{-3}	20

The SAW resonators with the N-DLC sensing layers were connected to a cascaded amplifier with two BFT25A transistors (Philips) and phase-shift circuits with two LC resonant networks to build the SAW sensor, as shown in Fig. 1(d). The sensing performance of the SAW gas sensor was characterized using a specially designed testing setup, as shown in Fig. 1(e) [19]. The sensor was put in a sealed testing chamber with a volume of 20 L. The temperature and the humidity in the test room were controlled at 25 ℃ and 50% unless otherwise specified by an air conditioner and a humidity controller to minimized temperature and humidity variations. The temperature and humidity in the test chamber were the same as those in the ambient environment, and the sensor was operated at 25 ℃ as well. High precision gas tight injectors (Hamilton) were used to collect the testing gases from gas sampling bags. The gas in sampling bags was collected from gas cylinders containing

the standard gases (NH_3, H_2, CO, NO, NO_2, H_2S, C_2H_5OH diluted to 2 vol% in dry air purchased from the National Institute of Measurement and Testing Technology, China). To measure the gas responses of the sensors, the collected gas in the injectors was injected into the testing chamber, and the gas concentration in the chamber was controlled by adjusting the injecting volume (0.01-10 ml). For example, with 0.1 ml NH_3 gas injected, the concentration of the test gas in the chamber is estimated to be 1 ppm. The response of the SAW sensor was defined as $\Delta f = f_s - f_0$, where f_s is the oscillating frequency of the sensor when exposed to the test gas, and f_0 is the oscillating frequency of the sensor in the ambient environment, respectively. The oscillating frequency of the SAW sensor was recorded using a frequency counter (Agilent 53210A). After the responses were recorded, the test gas was pumped out and pure air was filled in the chamber to allow the full recovery of the sensor.

An optical microscope (MV3000) was used to take the images of the SAW resonator. Electrical conductivity of the sensing layers was measured based on a four-probe method using a digital source meter (Keithley 2400). Surface morphology and thickness of the IDTs and N-DLC films were characterized using a field-emission scanning electron microscope (SEM, FEI Inspect F). Chemical composition and bonding structures of the films were analyzed using an X-ray photoelectron spectroscopy (XPS, Quantum 2000 Scanning ESCA Microprobe instrument) with a monochromatic Al Kα source (1486.6 eV) and a Raman spectroscopy (WITec Alpha 300R, 532 nm) respectively. The bonding of the films was studied using a vacuum

Fourier transform infrared (FTIR) spectrometer (Nicolet 6700) with a wavelength range of 1250-3750 cm^{-1}.

3. Results and discussion

3.1. Characterization of N-doped DLC films

The SEM images of N-DLC films are shown in Figs. 2(b)-2(d), which show the particulate features. Compared with those of other films, more pores can be found for the film #3, indicating that more N elements incorporated into the DLC film will lead to a more porous structure. This porous structure is beneficial for gas adsorption and diffusion in the application of gas sensing material. The inset in Fig. 2(d) shows the cross-sectional image of films, indicating the thickness of the N-DLC films is ~500 nm. As the thickness of individual film does not vary apparently, we present here only the result for the reference sample.

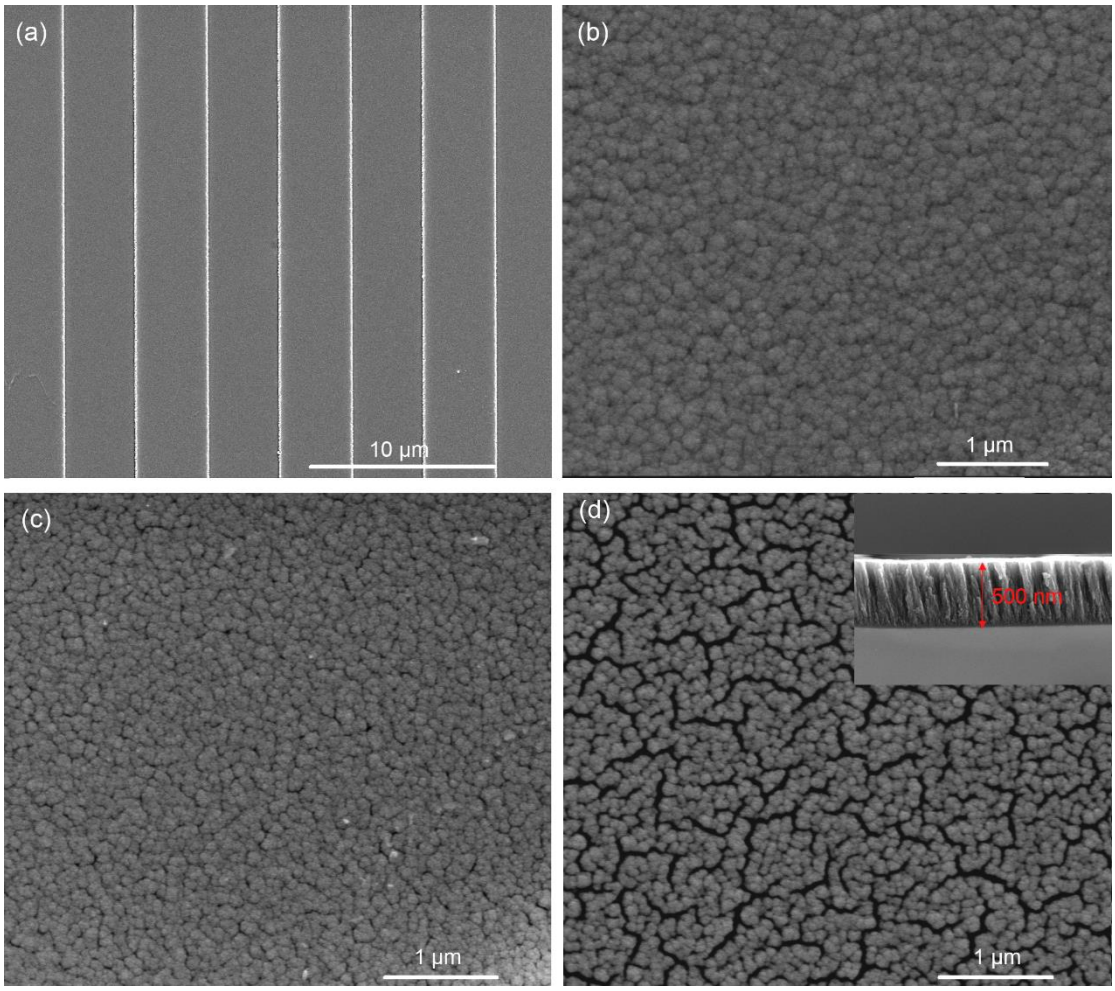

Fig. 2 SEM images of IDTs (a) and N-DLC films #1 (b), #2 (c), #3 (d) deposited on the quartz substrates. The inset in (d) is the cross-sectional image of the film #3, indicating the thickness is ~500 nm.

Raman spectra of the above three films are presented in Fig. 3. A wide IR band ranging from 850 to 1850 cm^{-1} (typically for DLC thin films) appears for all samples. Raman scattering of DLC can be deconvoluted into graphite (G) and disorder (D) bands at approximately 1550 cm^{-1} and 1360 cm^{-1}, respectively [30]. Both peaks in the spectra are broad and typical for amorphous carbon structures. The I_D/I_G, the ratio of integral area under D and G bands, is closely related to sp^3/sp^2 ratio in film. The I_D/I_G values are 0.80, 0.75, and 0.71 for the DLC films prepared under N_2 gas flow rate of 5, 15 and 30 sccm. The I_D/I_G intensities are decreased with the increased nitrogen doping, suggesting that the carbon substituted by a small amount of nitrogen would increase the sp^2 ratio of the film.

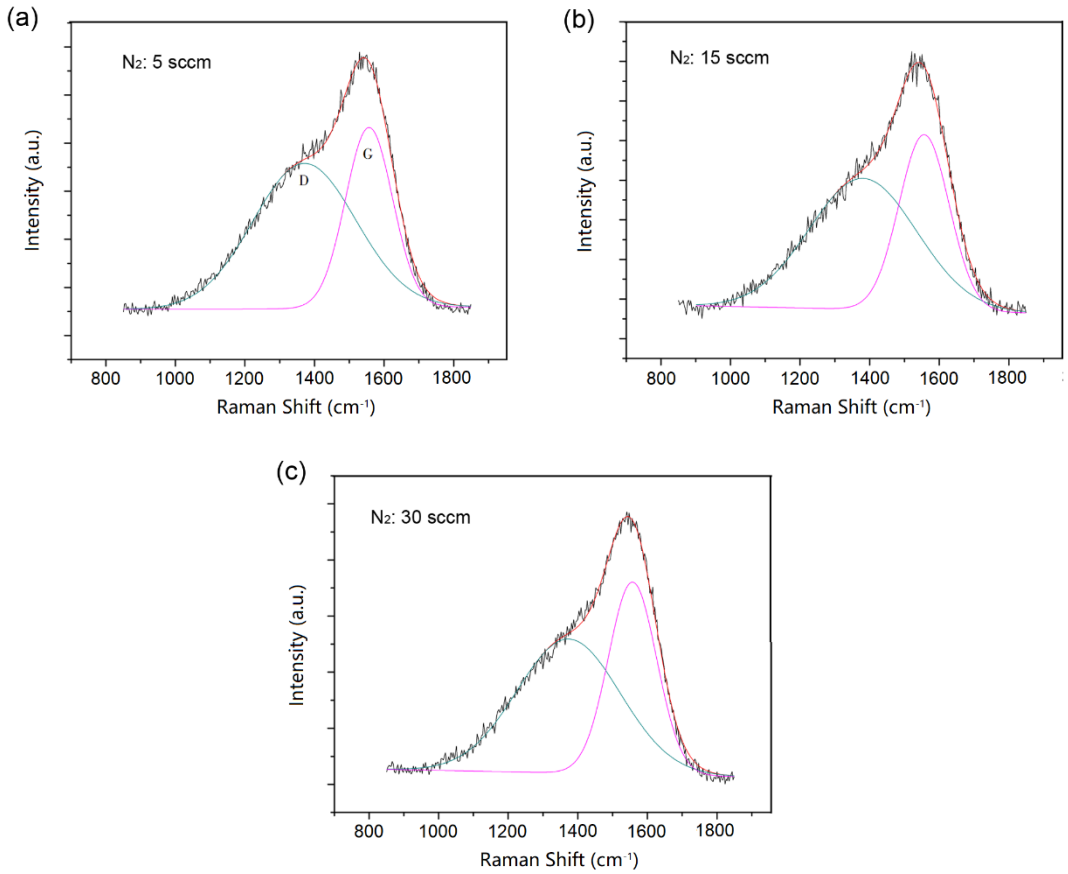

Fig. 3 Raman spectra of the prepared films #1 (a), #2 (b) and #3 (c).

Fig. 4(a) shows the XPS spectra of the N-DLC films. The intensity of N1s spectrum increases significantly with the increased N_2 flow rate, indicating that more N atoms are incorporated in the DLC film. Oxygen is also observed in the films, mainly due to exposure of the samples in ambient air before XPS measurement. Figs. 4(a) and 4(b) show the deconvoluted C1s and N1s spectra of the film #2. The C1s peak can be fitted with three sub-peaks: the main peak at 284.7 eV corresponds to the C-C sp^2 structure. The other peaks centered at 285.7 and 287.9 eV correspond to C-C sp^3 and C-N bonds, respectively [31,32]. The N1s spectra show two peaks at 399.6 and 400.5 eV which can be attributed to sp^3 C-N and sp^2 C-N bonds, respectively [31,32].

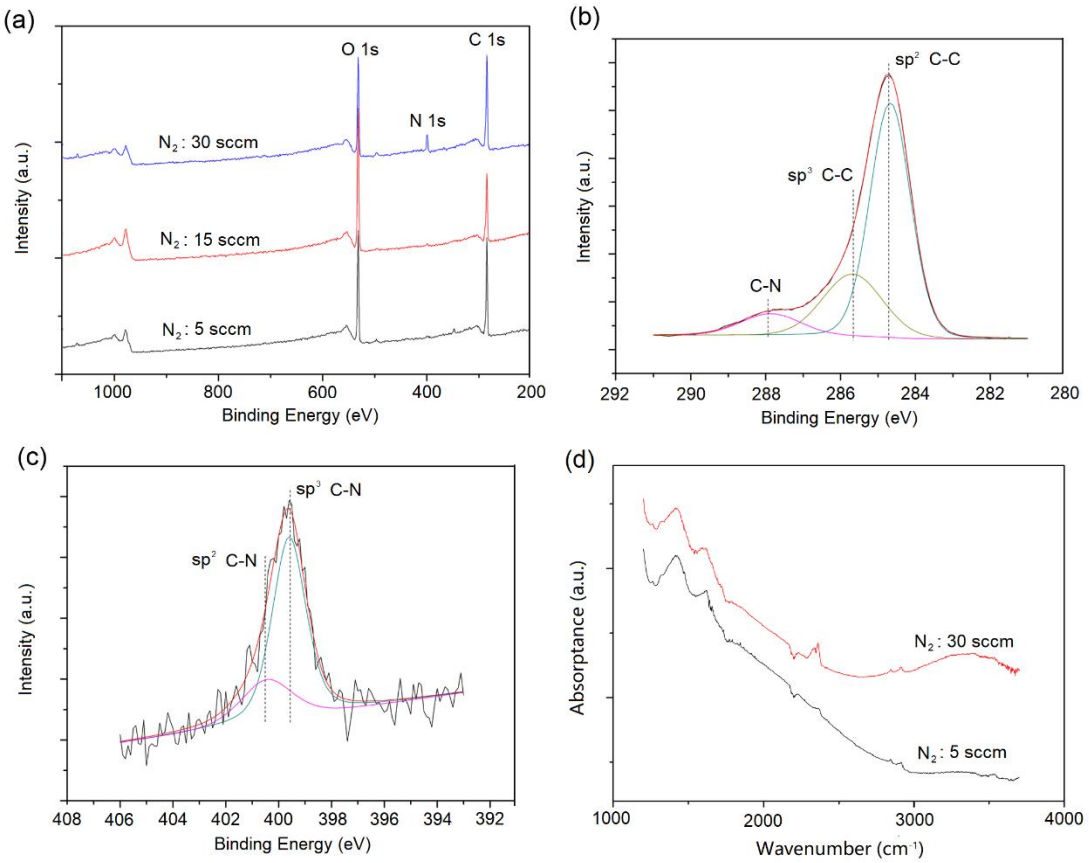

Fig. 4 (a) XPS spectra of prepared N-DLC films. Deconvoluted C1s (b) and N1s (c) spectra of the film #2. (d) FTIR spectra of the films #1 and #3 on quartz substrates.

Fig. 4d shows the FTIR spectra of the films #1 and #3 on quartz substrates in the range 1250-3750 cm^{-1}. In this figure, a few peaks belonged to the FTIR characteristics of N-DLC films are observed. Peaks in the range of 2800-3050 cm^{-1} are assigned to the C-H bonds [32]. With the increase of N_2 flow rate from 5 to 30 sccm, an obviously broad band between 3200 and 3600 cm^{-1} appears, revealing the formation of NH_x (x=1,2) bonds [33]. Peaks between 1300 and 1750 cm^{-1} are associated with the stretching vibration of both double and single carbon-nitrogen and carbon-carbon bonds. The peaks between 1600 and 1682 cm^{-1} are assigned to the sp^2 C=N bonds [34]. Moreover, no significant peak assigned to C≡N triple stretching bond is seen

around 2200 cm^{-1} in Fig. 4(d). The results from both XPS and FTIR spectra indicate that the carbon and nitrogen atoms in the nitrogen-doped DLC film are mainly existed as single C-N and double C=N bonds.

3.2. Gas sensing performance and sensing mechanism

Before the gas sensing test, the SAW sensor was firstly put into a test chamber with a constant temperature (25 ℃) and humidity (RH = 50%) to evaluate its noise level. Fig. 5(a) shows that the frequency signals of the sensor with the film #3 are fluctuated less than ±10 Hz, i.e. 0.1 ppm, in a period of 10000 s, indicating the low noise feature of the sensor.

The typical responses of the SAW sensors with N-DLC films toward 10 ppm NH_3 gas are shown in Fig. 5(b). All the sensors show positive responses, while the sensor with the film #3 has the highest response, which is ~6.7 kHz. In addition, the response times and recovery times of these sensors are similar, which are 5±0.5 s and 29±1.5 s, respectively. Previous studies [15,19] reported that there are three major changes of the sensing films after adsorption of the gases, i.e., the changes of sheet conductivity ($\Delta\sigma_s$), areal density ($\Delta\rho_s$) and elastic modulus (ΔE), all of which will lead to the response of a SAW based gas sensor.

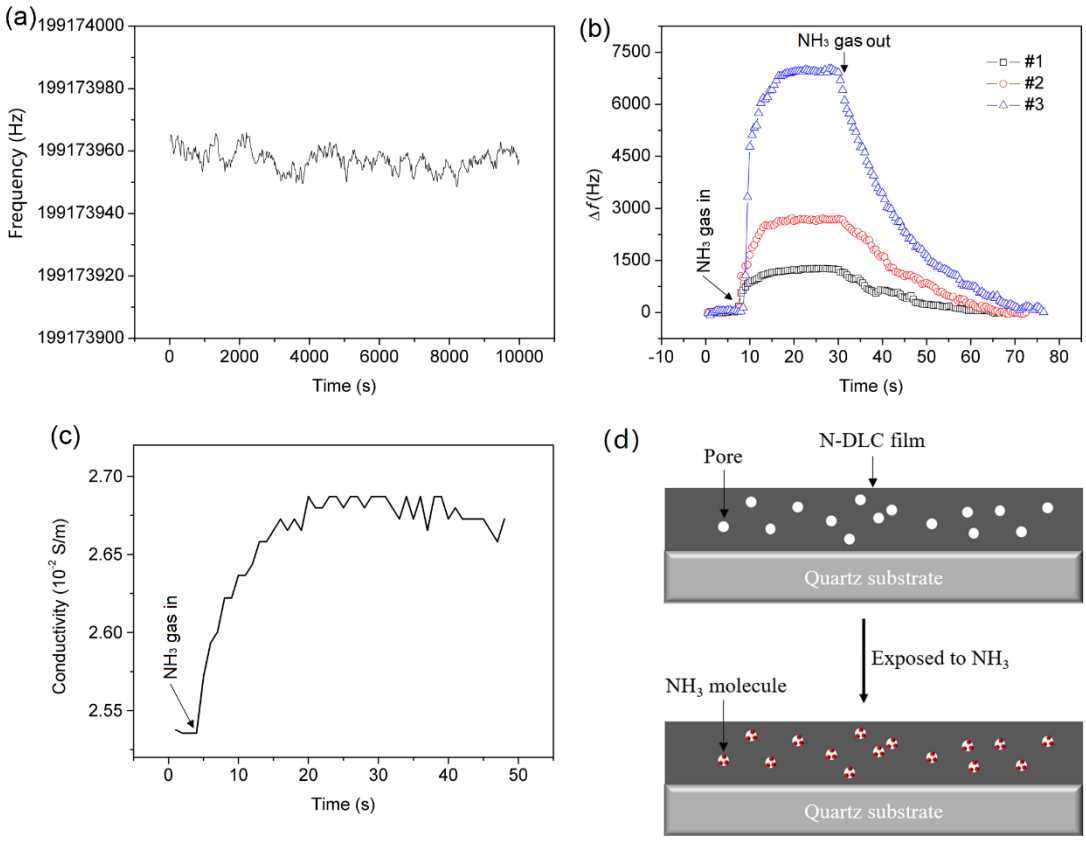

Fig. 5 (a) The frequency signals of the sensor in a constant environment within 10000 s; (b) Dynamic frequency responses of SAW sensors with three different films toward 10 ppm NH_3; (c) Dynamic changes of electrical conductivity of the film #3 when exposed to 10 ppm NH_3; (d) Proposed NH_3 sensing mechanism of N-doped DLC film. Pores in the film can trap the NH_3 molecules, thus resulting the decreased porosity of the film.

The changes of conductivity, $\Delta\sigma_s$, affects the response (Δf) of a SAW gas sensor, which can be described using the following equation [15,19]:

$$\Delta f = -f_0 \times \frac{K^2}{2} \times \Delta\left(\frac{1}{1+\left(\frac{v_0 c_s}{\sigma_s}\right)^2}\right) \quad (1)$$

where f_0 (=200 MHz) and v_0 (=3158 m/s) are the unperturbed frequency and SAW velocity of the sensor, K^2 (= 0.0011, or 0.11%) is the electromechanical coupling

coefficient of ST-cut quartz substrate taken from Ref. [35], C_s= 0.5 pF/cm is the capacitance per unit length measured by a network analyzer (Agilent E5071C). When exposed to 10 ppm NH_3, the σ_s value of the film #3 is increased by ~6%, as shown in Fig. 5(c). Based on these results, the response caused by $\Delta\sigma_s$ is calculated to be less than 0.1 Hz, which is far less than the measured response (~ 6.7 kHz). Therefore, it can be assumed that the change of sheet conductivity is not the key reason for the measured responses of the SAW sensors toward NH_3 gas.

FTIR characterization has revealed that there are polar groups (NH_x) on the N-DLC films. Previous studies have reported that these polar groups can act as the active sites for the adsorption of NH_3 molecules [27]. The adsorbed NH_3 gas molecules can lead to increases of both areal density ($\Delta\rho_s$) and modulus of the N-DLC films by filling the pores in the sensitive films [36], as illustrated in Fig. 5(d). The areal density ($\Delta\rho_s$) and elastic modulus cause the responses (Δf) of the SAW sensor, which follows the Equation below [15,19]:

$$\Delta f = C_e f_0 h \Delta\left(\frac{4u}{v_0^2}\times\frac{u+\lambda}{u+2\lambda}\right)+C_m\times f_0^2\times\Delta\rho_s \quad (2)$$

Where μ and λ are the shear and bulk modulus of elasticity of the sensitive films, C_e and C_m are the sensitivity coefficients of elasticity and mass respectively, h is the thickness of the film.

Equation (2) can also be written in terms of change in Young's modulus (ΔE) and mass (Δm) of the sensitive film due to adsorption of NH_3 gas as [36],

$$\Delta f = p\Delta E\text{-}q\Delta m \quad (3)$$

Where p and q are positive constants incorporating all the other constants. Based on the Equation (3), the increases of modulus (ΔE) and mass (Δm) of films caused by the adsorbed NH_3 gas molecules will result in positive and negative frequency shifts of SAW sensors, respectively, and the measured responses are the summation of the two positive and negative frequency shifts. From Figs. 5-7, it can be clearly seen that all the measured responses toward NH_3 gas with different concentrations are positive, which indicates that the positive frequency shifts caused by the increased modulus (ΔE) are stronger than the negative frequency shifts caused by the increased mass (Δm) in all cases [36-38].

Although all the SAW sensors with the N-DLC films are based on the same sensing mechanism as discussed above, Fig. 5(b) reveals that the sensor coated with the film #3 has shown the best sensitivity. The differences among the sensing performances of the sensors could be attributed to the different microstructures of the sensing layer materials. The FTIR results revealed that the film #3 has more active NH_x groups on its surface for the adsorption of NH_3 molecules. In addition, higher N content in the film would lead to higher porosity of the N-DLC film, as confirmed by the SEM results shown in Fig. 2(d) [28]. As a result, when the film with a higher N content was exposed to NH_3, more NH_3 molecules were adsorbed to fill the pores in the film, thus leading to much more significant decrease of the porosity. Consequently, the modulus was significantly increased. This result indicates the possibility of adjusting the sensitivity of a SAW gas sensor by tuning the total pore volume and pore size in the sensing film.

For the following measurements, we will use the sensor with the film #3 to study its sensing performance in more detail. Fig. 6(a) shows the dynamic response of the sensor toward NH_3 gas with the concentration ranged from 100 ppb to 100 ppm. It can be observed that the sensor has a response of ~0.65 kHz to 100 ppb NH_3 gas, and the response can be as large as ~22.5 kHz when the NH_3 concentration is increased to 100 ppm. In addition, it is worthwhile to note (Fig. 6(b)) that the logarithmic of response (log Δf) is linear related to the logarithmic of the concentration of NH_3 gas (log C), which can be used for determine the responses of the sensor toward any concentrations of NH3 gas in the range from 100 ppb to 100 ppm. The sensor has short response and recovery times, which are ~5 s and ~29 s, respectively, which remain nearly constants with the change of the NH_3 gas concentration. These response and recovery times are much shorter than those previously reported SAW NH_3 gas sensors [39-43], which were usually more than 30 s, as listed in Table 2. The excellent sensitivity, linearity between the log Δf and log C, and fast response/recovery make this sensor more appropriate for the practical applications.

Table 2 Comparisons of sensing performance of SAW NH_3 sensor based on various sensing materials

Working frequency (MHz)	Sensing material	NH_3 concentration (ppm)	Response (kHz)	Response/Recovery time (s)	Ref.
162	Au-poly(vinyl) alcohol	2	-0.9	60/Not Know	[39]
200	SnO_2-SiO_2	3	2	100/200	[40]

200	Graphene oxide	1	1.8	80/500	[41]
200	SiO_2-TiO_2	1	2	75/55	[42]
114.7	poly-N-vinylpyrrolidone	120	-0.83	50/40	[43]
200	N-DLC	2	6.6	5/29	Present work

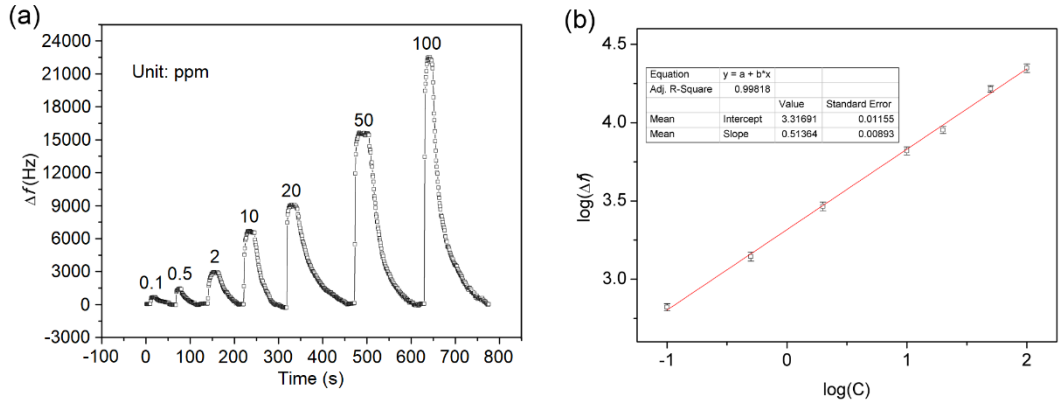

Fig. 6 (a) Dynamic responses of the SAW sensor with the film #3 to NH_3 with different concentrations; (b) The logarithmic of response (log Δf) as a function of logarithmic of the concentration of NH_3 gas (log C).

The sensor's dynamic responses to C_2H_5OH, H_2S, H_2, CO, NO_2 and NO were further measured to investigate the selectivity of the sensor. Result shows that the sensor has no noticeable responses toward H_2S, H_2, CO, NO_2 and NO gases. It has a response towards C_2H_5OH gases and this response can be attributed to the adsorption of the C_2H_5OH molecules on the active polar sites. However, its response is much weaker than that to NH_3, as shown in Fig. 7(a), indicating the excellent selectivity of the sensor toward NH_3 gas.

For a practical sensor, both good short-term reproducibility and long-term stability are critical, and the stability of a SAW sensor is highly dependent on the stability of the sensing film used. The short-term reproducibility of the sensor was

investigated by conducting four consecutive sensing tests in 5 minutes, and the obtained results are shown in Fig. 7(b). The results show excellent short-term reproducibility of the sensor since the response curves are nearly same for the four individual tests, which confirms that the N-DLC sensing film is highly recoverable. The long-term stability of the sensor was further investigated by conducting the sensing test every 10 days within a 90-day period, and the results are shown in Fig. 7(c). The sensor shows the similar responses to 0.5 ppm, 10 ppm and 100 ppm NH_3, respectively, in the four different tests within 90 days, indicating the good long-term stability of the sensor. The good long-term and short-term stability may be derived from the excellent physical and chemical stability of the N-DLC film.

It is well-known that the polar groups on the N-DLC film can also be the active sites for the adsorption of polar H_2O molecules. Hence, the relative humidity (RH) may influence the sensing performance of the sensor toward NH_3 gas. To verify this influence, we have investigated the sensing performance of the sensor under different RHs. As shown in Fig. 7(d), the baseline of the sensor is shifted by -19.8 and -30.3 kHz, when the RH is increased from 10% to 50% and 80%, respectively. These negative shifts confirm that there are more H_2O molecules adsorbed on the film at higher RHs, which leads to an increased weight of the sensing film. The sensor's responses toward 50 ppm NH_3 gas under RH = 10%, 50% and 80% are 20.4, 17.1 and 14.7 kHz, respectively. Interestingly, the frequency responses show only moderate decrease with the increased RH value, which might be caused by the increased amount of H_2O molecules occupying the active polar groups. With this result, it can

be confirmed that this sensor can be used for NH_3 detection at different environments with different RH values.

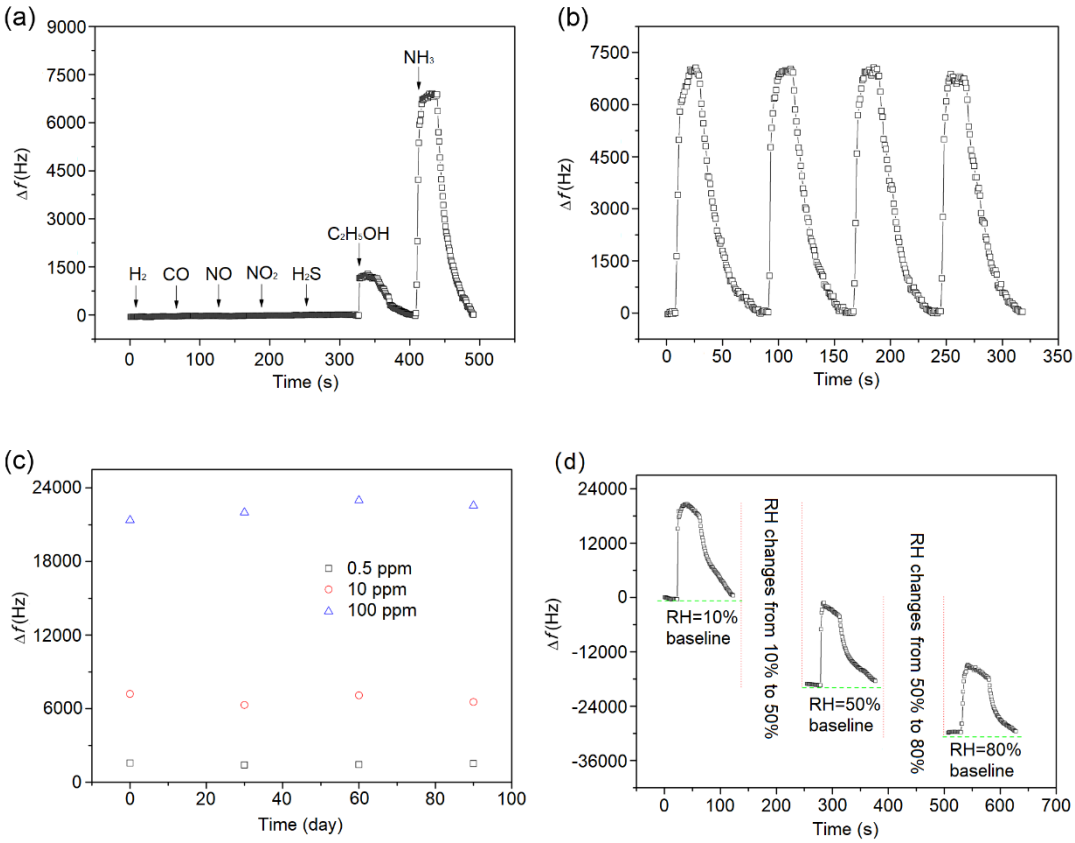

Fig. 7 (a) The dynamic responses of the sensor with the film #3 to 10 ppm H_2, CO, NO, NO_2, H_2S, C_2H_5OH and NH_3 gases; (b) The dynamic responses of the sensor to 10 ppm NH_3 for four consecutive cycles; (c) The responses of the sensor to 0.2, 10 and 100 ppm NH_3 within 90 days; (d) Dynamic responses of the sensor to 50 ppm NH_3 under environments with different RHs.

4. Conclusion

In this paper, the NH_3 gas sensing performance of quartz SAW sensors with the N-DLC films as sensing layers were investigated. The porous structure and the active polar groups on the N-DLC film were beneficial for the NH_3 gas sensing application. The sensor was able to *in-situ* detect NH_3 concentrations in a range from 100 ppb to 100 ppm with fast response and recovery. The good physical and chemical inertness of the films ensure the excellent reproducibility and stability of the sensor. The sensing mechanism of the sensor was attributed to the decreased porosity of the film caused by adsorbed NH_3 molecules, which lead to an increase of the elastic modulus of the sensitive film. The high sensitivity, excellent linearity, selectivity, fast response, recovery and excellent stability of the sensor make it highly potential for practical applications.

Acknowledgements

This work was supported by the Fundamental Research Funds for the Central Universities (2682019CX68), the Scientific Research Foundation of SWJTU (A1920502051907-2-032), the National Natural Science Foundation of China (51902272), the UK Engineering and Physical Sciences Research Council (EPSRC) grants EP/P018998/1, Newton Mobility Grant (IE161019) through Royal Society and the National Natural Science Foundation of China.

Declaration of interests

The authors declare no conflicts of interests.

References

[1] S. Sriram, V. Nagarajan, R. Chandiramouli, H_2S and NH_3 adsorption characteristics on CoO nanowire molecular device-A first-principles study, Chem. Phys. Lett. 636 (2015) 51-57.

[2] S. Li, A. Liu, Z. Yang, J. Wang, F. Liu, R. You, J. He, C. Wang, X. Yan, P. Sun, X. Liang, G. Lu, Design and preparation of the WO_3 hollow spheres@ PANI conducting films for room temperature flexible NH_3 sensing device, Sens. Actuat. B Chem. 289 (2019) 252-259.

[3] J. Guo, W.S. Xu, Y.L. Chen, A.C. Lua, Adsorption of NH_3 onto activated carbon prepared from palm shells impregnated with H_2SO_4, J. Colloid Interf. Sci. 281 (2005) 285-290.

[4] Y. Wang, J. Liu, X. Cui, Y. Gao, J. Ma, Y. Sun, P. Sun, F. Liu, X. Liang, T. Zhang, G. Lu, NH_3 gas sensing performance enhanced by Pt-loaded on mesoporous WO_3, Sens. Actuat. B Chem. 238 (2017) 473-481.

[5] B. Timmer, W. Olthuis, A. Van Den Berg, Ammonia sensors and their applications-a review, Sens. Actuat. B Chem. 107(2005) 666-677.

[6] J. Skřínský, J. Vereš, J. Trávníčková, D. Andrea, Explosions caused by corrosive gases/vapors, Materials Science Forum. Trans Tech Publications Ltd. 844 (2016) 65-72.

[7] Y. Li, M. Bi, B. Li, L. Huang, W. Gao, Explosion hazard evaluation of renewable hydrogen/ammonia/air fuels, Energy 159 (2018) 252-263.

[8] U.J. Pfahl, M.C. Ross, J.E. Shepherd, K.O. Pasamehmetoglu, C. Unal,

Flammability limits, ignition energy, and flame speeds in H_2–CH_4–NH_3–N_2O–O_2–N_2 mixture, Combust. Flame 123 (2000) 140-158.

[9] Y. Xiong, W. Xu, D. Ding, W. Lu, L. Zhu, Z. Zhu, Y. Wang, Q. Xue, Ultra-sensitive NH_3 sensor based on flower-shaped SnS_2 nanostructures with sub-ppm detection ability, J. Hazard. Mater. 341 (2018) 159-167.

[10] D. Deng, B. Gao, C. Zhang, X. Duan, J. Ning, Investigation of protic NH4SCN-based deep eutectic solvents as highly efficient and reversible NH_3 absorbents, Chem. Eng. J. 358 (2019) 936-943.

[11] B. Xiao, Y. Li, X. Yu, J. Chen, MXenes: Reusable materials for NH_3 sensor or capturer by controlling the charge injection, Sens. Actuat. B: Chem. 235 (2016) 103-109.

[12] T.H. Kim, D.K. Nandi, R. Ramesh, S.M. Han, B. Shong, S.H. Kim, Some Insights into Atomic Layer Deposition of MoN_x Using $Mo(CO)_6$ and NH_3 and Its Diffusion Barrier Application, Chem, Mater. 31 (2019) 8338-8350.

[13] I. Voiculescu, A.N. Nordin, Acoustic wave based MEMS devices for biosensing applications, Biosens. Bioelectron. 33 (2012): 1-9.

[14] M. Penza, P. Aversa, G. Cassano, W. Wlodarski, K. Kalantar-Zadeh, Layered SAW gas sensor with single-walled carbon nanotube-based nanocomposite coating, Sens. Actuat. B Chem. 127 (2007) 168-178.

[15] Y. Tang, X. Xu, S. Han, C. Cai, H. Du, H. Zhu, X. Zu, Y. Fu, ZnO-Al_2O_3 nanocomposite as a sensitive layer for high performance surface acoustic wave H2S gas sensor with enhanced elastic loading effect, Sens. Actuat. B Chem. 304 (2020)

127395.

[16] S. Tadigadapa, K. Mateti, Piezoelectric MEMS sensors: state-of-the-art and perspectives, Meas. Sci. Technol. 20 (2009) 092001.

[17] M.C. Chiang, H.C. Hao, C.Y. Hsiao, S.C. Liu, C.M. Yang, K.T. Tang, D.J. Yao, Gas sensor array based on surface acoustic wave devices for rapid multi-detection, 2012 IEEE Nanotechnology Materials and Devices Conference (NMDC2012). IEEE, 2012: 139-142.

[18] T.H. Lin, Y.T. Li, H.C. Hao, I.C. Fang, D.J. Yao, Surface acoustic wave gas sensor for monitoring low concentration ammonia, 2011 16th International Solid-State Sensors, Actuators and Microsystems Conference. IEEE, 2011: 1140-1143.

[19] Y. Tang, W. Wu, B. Wang, X. Dai, W. Xie, Y. Yang, R. Zhang, X. Shi, H. Zhu, J. Luo, Y. Guo, X. Xiang, X. Zu, Y. Fu, H_2S gas sensing performance and mechanisms using CuO-Al_2O_3 composite films based on both surface acoustic wave and chemiresistor techniques, Sens. Actuat. B Chem. 325 (2020) 128742.

[20] I. Constantinoiu, D. Miu, C. Viespe, Surface Acoustic Wave Sensors for Ammonia Detection at Room Temperature Based on SnO_2/Co_3O_4 Bilayers, J. Sensors 2019 (2019) 1-6.

[21] A. Dey, Semiconductor metal oxide gas sensors: A review, Mater. Sci. Eng. B 229 (2018) 206-217.

[22] C. Wei, L. Dai, A. Roy, T.B. Tolle, Multifunctional chemical vapor sensors of aligned carbon nanotube and polymer composites, J. Am. Chem. Soc. 128 (2006)

1412-1413.

[23] O. Sharifahmadian, F. Mahboubi, A. Oskouie, Structural evolution and tribological behavior of nitrogen-doped DLC coatings deposited by pulsed DC PACVD method, Diam. Relat. Mater. 91 (2019) 74-83.

[24] X. Yan, T. Xu, G. Chen, H. Liu, Study of structure, tribological properties and growth mechanism of DLC and nitrogen-doped DLC films deposited by electrochemical technique, Appl. Surf. Sci. 236 (2004) 328-335.

[25] W. Zhang, Y. Xia, J. Ju, L Wang, Z Fang, M Zhang, Electrical conductivity of nitride carbon films with different nitrogen content, Solid State Commun. 126 (2003) 163-166.

[26] R.Z. Moghadam, H.R. Dizaji, M.H. Ehsani, Modification of optical and mechanical properties of nitrogen doped diamond-like carbon layers, J. Mater. Sci.-Mater. El. 2019, 30(22): 19770-19781.

[27] A.V. Kiselev, Y.I.Yashin, Gas-adsorption chromatography, Springer, 2013.

[28] P. Hammer, R.G. Lacerda, R. Droppa Jr, F. Alvarez, Comparative study on the bonding structure of hydrogenated and hydrogen free carbon nitride films with high N content, Diam. Relat. Mater. 9 (2000) 577-581.

[29] Xie D, Liu H, Deng X, Y.X. Leng, N. Huang, Deposition of aC: H films on UHMWPE substrate and its wear-resistance, Appl. Surf. Sci. 256 (2009) 284-288.

[30] S. Srinivasan, Y. Tang, Y.S. Li, Q. Yang, A. Hirose, Ion beam deposition of DLC and nitrogen doped DLC thin films for enhanced haemocompatibility on PTFE, Appl. Surf. Sci. 258 (2012) 8094-8099.

[31] T.W. Scharf, R.D. Ott, D. Yang, J. A. Barnard, Structural and tribological characterization of protective amorphous diamond-like carbon and amorphous CNx overcoats for next generation hard disks, J. Appl. Phys. 85 (1999) 3142-3154.

[32] E. Riedo, F. Comin, J. Chevrier, F. Schmithusen, S. Decossas, M. Sancrotti, Structural properties and surface morphology of laser-deposited amorphous carbon and carbon nitride films, Surf. Coat. Tech. 125 (2000) 124-128.

[33] T. Heitz, B. Drevillon, C. Godet, J.E. Bourée, Quantitative study of C-H bonding in polymerlike amorphous carbon films using in situ infrared ellipsometry, Phys. Rev. B 58 (1998) 13957.

[34] T. Szörényi, C. Fuchs, E. Fogarassy, J. Hommet, F. Le Normand, Chemical analysis of pulsed laser deposited a-CNx films by comparative infrared and X-ray photoelectron spectroscopies, Surf. Coat. Tech. 125 (2000) 308-312.

[35] D.S. Ballantine Jr., S.J. Martin, A.J. Ricco, G.C. Frye, H. Wohltjen, R.M. White, E.T.Zellers, Acoustic Wave Sensors: Theory, Design, and Physico-Chemical Applications, Academic Press, San Diego, 1997.

[36] V.B. Raj, H. Singh, A.T. Nimal, M.U. Sharma, M. Tomar, V. Gupta, Distinct detection of liquor ammonia by ZnO/SAW sensor: Study of complete sensing mechanism, Sens. Actuat. B Chem. 238 (2017) 83-90.

[37] V.B. Raj, A.T. Nimal, Y. Parmar, M.U. Sharma, V. Gupta, Investigations on the origin of mass and elastic loading in the time varying distinct response of ZnO SAW ammonia sensor, Sens. Actuat. B Chem. 166 (2012) 576-585.

[38] S.H. Wang, C.Y. Shen, Z.J. Lien, J.H. Wang, Nitric oxide sensing properties of a

surface acoustic wave sensor with copper-ion-doped polyaniline/tungsten oxide nanocomposite film, Sens. Actuat. B Chem. 243 (2017) 1075-1082.

[39] M. Šetka, F.A. Bahos, D. Matatagui, Z. Kral, S. Vallejos, Polypyrrole based love-wave gas sensor devices with enhanced properties to ammonia, Multidisciplinary Digital Publishing Institute Proceedings. 2 (2018) 786.

[40] Y.J. Guo, G.D. Long, Y.L. Tang, J.L. Wang, Q.B. Tang, X.T. Zu, J.Y. Ma, B. Du, H. Torun, Y.Q. Fu, Surface acoustic wave ammonia sensor based on SiO_2–SnO_2 composite film operated at room temperature, Smart Mater. Struct. 29 (2020) 095003.

[41] Q.B. Tang, Y.J. Guo, Y.L. Tang, G.D. Long, J.L. Wang, D.J. Li, X.T. Zu, J.Y. Ma, L. Wang, H. Torun, Y.Q. Fu, Highly sensitive and selective Love mode surface acoustic wave ammonia sensor based on graphene oxides operated at room temperature, J. Mater. Sci. 54 (2019) 11925-11935.

[42] Y. Tang, D. Ao, W. Li, X. Zu, S. Li, Y. Fu, NH_3 sensing property and mechanisms of quartz surface acoustic wave sensors deposited with SiO_2, TiO_2, and SiO_2-TiO_2 composite films, Sens. Actuat. B Chem. 254 (2018) 1165-1173.

[43] T.H. Lin, Y.T. Li, H.C. Hao, C.M. Yang, I.C. Fang, D. J. Yao, Surface acoustic wave gas sensor for monitoring low concentration ammonia, 2011 16th International Solid-State Sensors, Actuators and Microsystems Conference. IEEE, 2011: 1140-1143.